PSFC/JA-10-18

Using mixed gases for massive gas injection disruption mitigation on Alcator C-Mod

Bakhtiari, M.*, Olynyk, G., Granetz, R., Whyte, D.G., Reinke, M.L., Zhurovich, K., Izzo, V.**

* University of Wisconsin–Madison. Current address: Roswell Park Cancer Institute, Buffalo, New York.
** University of California, San Diego, California.

August 2010

Plasma Science and Fusion Center
Massachusetts Institute of Technology
Cambridge MA 02139 USA

This work was supported by the U.S. Department of Energy, Grant No. DE-FG02-04ER54762 and U.S. Department of Energy Cooperative Agreement DE-FC02-99ER54512. Additional support provided by NSERC Canada PGS M program. Reproduction, translation, publication, use and disposal, in whole or in part, by or for the United States government is permitted.

Submitted for publication to *Nuclear Fusion*.

Using mixed gases for massive gas injection disruption mitigation on Alcator C-Mod

M Bakhtiari[1], G Olynyk[2]‡, R Granetz[2], D G Whyte[2], M L Reinke[2], K Zhurovich[2], and V Izzo[3]

[1] University of Wisconsin–Madison, Madison, Wisconsin, USA§
[2] Plasma Science and Fusion Center, Massachusetts Institute of Technology, Cambridge, Massachusetts, USA
[3] University of California, San Diego, California, USA

E-mail: golynyk@mit.edu

Abstract. Mixed gases are used for massive gas injection disruption mitigation on Alcator C-Mod in order to optimize radiation efficiency, halo current reduction, and response time. Gas mixtures of helium and argon (argon fraction 0–50%) are investigated in detail, as well as mixtures of deuterium, argon, krypton, and helium. Experiments show that injecting He/Ar mixtures leads to faster thermal and current quenches than with pure helium or argon injection, thus improving the time response of the disruption mitigation system and reducing the halo current. Small fractions of argon (∼5–10%) in helium also lead to optimized radiation fractions with large electron density increases in the core plasma. These results are consistent with the expectation that small fractions of argon will be entrained with the faster helium in the early phases of gas flow. The gas mixing allows one to simultaneously exploit the fast particle delivery rate of light helium gas and the large radiation capability of argon.

PACS numbers: 28.52.-s, 51.10.+y, 52.25.Vy, 52.25.Ya, 52.55.Fa

Submitted to: *Nuclear Fusion*

‡ to whom correpondence should be addressed.
§ current address: Roswell Park Cancer Institute, Buffalo, New York, USA

1. Introduction

In a tokamak, disruptions are the sudden loss of energy confinement caused by the destruction of magnetic surfaces. The sudden in plasma resistivity associated with the rapidly falling temperature results in a fast current decay and dissipation of the plasma's thermal and poloidal magnetic energy. Disruptions have deleterious effects through intense localized heat flux to plasma facing components, generation of halo current in the conducting vessel, and the generation of significant current carried in multi-MeV runaway electrons that are eventually lost into plasma facing components. Preventing or mitigating their occurence will be a requirement for any reactor-regime tokamak [1].

The principle of massive gas injection (MGI) disruption mitigation is to force a rapid and comparatively benign release of the plasma energy through a forced injection of a radiative species into the plasma [2]. Massive gas injections also have the potential to prevent runaway electron formation by creating a strong collisional drag force [3], induced MHD stochasticity [4, 5], and strong bremsstrahlung and synchrotron radiation drag [6]. Noble gas species are used because they have low chemical reactivity with in-vessel components, which are often at elevated temperatures.

The location of the gas reservoir and fast valve is an important design consideration for MGI systems. For maintenance access and to avoid radiation damage, it is likely that the reservoir and valve for a burning plasma experiment such as ITER will be located outside the neutron shielding and toroidal field coil set, 3–5 m from the plasma edge. This raises concerns about the overall response time of the mitigation system. A signal can be immediately sent to open the disruption mitigation valve when triggered by a disruption detection system, but the delivery of the radiative species to the plasma is delayed by the time it takes the gas to travel down the pipe from the valve to the plasma edge.

Therefore, it would appear that light gases such as H_2 or He, with high gas sound speeds, would be favored since they will propagate the fastest to the plasma edge [7]. However, light, low atomic number (low-Z) impurities have low radiation rate coefficients due to their full ionization in the plasma, which can reduce the effectiveness of the disruption mitigation [8]. On the other hand, heavy, high-Z gases have high radiation rate coefficients due to their large number of bound electrons, but will move more slowly to the plasma, introducing an undesirable delay to the initiation of plasma cooling [9].

Previous disruption mitigation experiments on the JT-60U tokamak using a conventional gas injection system ($\sim$ 100 times smaller injection rate than with massive gas injection systems) showed that gas mixtures of low-Z and high-Z noble gases resulted in larger radiated power and a larger density increment, which helped decrease runaway electron formation [9, 10, 11].

We report here on the use of gas mixtures with the massive gas injection disruption mitigation system on Alcator C-Mod [8]. In section 2 we discuss the requirements for disruption mitigation and discuss the benefits of using gas mixtures. In section 3

we present the results of experiments on C-Mod using a helium/argon mixture, showing that disruption mitigation can be optimized with respect to the argon gas fraction. We also present observations of massive gas injection using mixtures of hydrogen/argon and helium/krypton. In section 4 we interpret the observations using a zero-dimensional radiation/ionization code in order to illuminate some of the physics behind the experimental results. Conclusions are given in section 5.

2. Requirements for disruption mitigation

For a disruption mitigation system to qualify as successful, the following three requirements must be met:

- The fast delivery of a large quantity of radiative species into the plasma. The delivery time must be faster than the growth time of the plasma instabilities that lead to the disruption through violation of the tokamak's operational limits (e.g. vertical displacement, locked-mode, pressure limit, etc.)
- Efficient energy removal and density increment during the thermal quench to prevent localized heat loads to plasma facing components, and to prevent runaway electron formation during the current quench.
- Rapid and resistive termination of the plasma current to minimize halo currents.

In the following subsections, the details of these requirements are discussed.

2.1. Gas delivery

For a given MGI system (plenum, valve, pipe), the delivery rate of the gas to the plasma is set by the gas sound speed. The speed of sound in a monatomic gas at a given temperature depends on the atomic mass M of the gas ($c_s \sim 1/M^{1/2}$). A summary of C-Mod disruption mitigation experiments using pure helium and argon gases [8] is shown in figure 1. Figure 1(a) indicates the effect of gas delivery speeds.

In C-Mod experiments the gas valve is located 2 m from the plasma edge. The gas travels through a stainless steel tube with 9.4 mm internal diameter (13.0 mm external diameter). The effective time response, which is desired to be as short as possible, is measured as the time between the valve opening, t_{inj} (as indicated by the start of the rise of the pressure waveform just downpipe from the valve), and the time of the beginning of the current quench, t_{CQ}, which indicates that the plasma has become cold and highly resistive. The overall response time for pure He injection is found to be $\sim 25\%$ better than for pure Ar injection. However, this relative advantage for He is far less than the ratio of sound speeds; c_s in He is approximately 3 times faster than in Ar. This indicates a competition between radiation efficiency and the speed of sound in the different gases. We now examine how we can exploit this competition by using mixed gases for disruption mitigation.

The particle delivery rate for pure gases can be assessed using a simple analytic model based on Euler's equation for adiabatic expansion without friction. We assume an infinitely large plenum located at $x < 0$. A fast valve located at $x = 0$ connects the

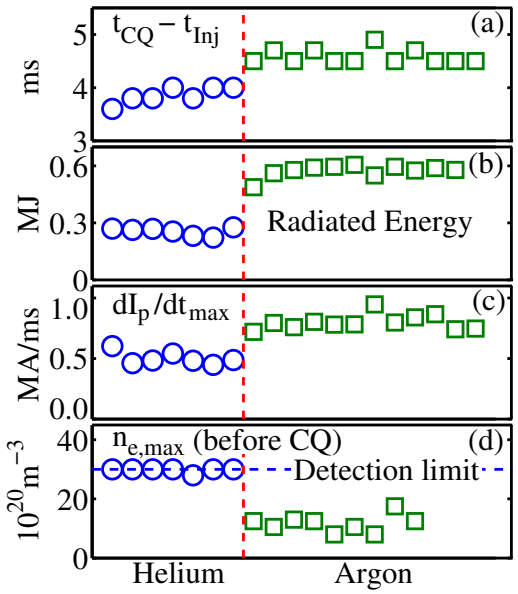

Figure 1. Summary of pure He and Ar gas-jet disruption mitigation experiments on Alcator C-Mod [8]. (a) Time delay from start of pressure rise in pipe to beginning of current quench, (b) radiated energy, (c) maximum rate of change of plasma current, (d) electron density n_e at beginning of current quench. Note n_e for helium MGI is at detection limits. Neither He nor Ar can fulfill all disruption mitigation requirements.

plenum to a constant-diameter pipe which runs from $x = 0$ to $x = L_p$, where L_p is the length of the pipe (m). At $x = L_p$, the pipe empties into a vacuum region of infinite volume. The sound speed of the gas in the plenum is given by:

$$c_0 = \sqrt{\frac{\gamma P_0}{\rho_0}} = \sqrt{\gamma R T_0} \tag{1}$$

where c is the sound speed ($\mathrm{m\,s^{-1}}$), γ is the ratio of specific heats, or adiabatic constant, P is the gas pressure (Pa), ρ is the mass density of the gas ($\mathrm{kg\,m^{-3}}$), $R = \bar{R}/M$ is the gas constant ($\mathrm{J\,kg^{-1}\,K^{-1}}$), and T is the gas temperature (K). The subscript 0 indicates the stagnation condition, assumed to be valid in the plenum where the velocity of the gas is always small.

If the valve opens at $t = 0$, the gas flows into the pipe (initially a vacuum), and a shock front develops. The evolving sound speed c and fluid velocity u as a function of x (distance down the pipe) and time t are given by [12]:

$$c = \frac{2}{\gamma+1} c_0 - \frac{\gamma-1}{\gamma+1}\frac{x}{t} \tag{2}$$

$$u = \frac{2}{\gamma+1} c_0 + \frac{2}{\gamma+1}\frac{x}{t} \tag{3}$$

Examination of (2) shows that at the pipe exit, $x = L_p$, the solution is physical ($c > 0$) only after a minimum elapsed time of:

$$\Delta t_0 \geq \frac{\gamma-1}{2}\frac{L_p}{c_0} \tag{4}$$

For an ideal monatomic gas, $\gamma = 5/3$. Thus, for noble gases, the minimum delay for gas particles to arrive is $\Delta t_0 = L_\mathrm{p}/3c_0$. The gas particle delivery rate into the infinite vacuum at $x = L_\mathrm{p}$ is given by:

$$\dot{N}\Big|_{x=L_\mathrm{p}} = (nu)_{x=L_\mathrm{p}} A \sim \left(\frac{\rho}{M} A\right) \tag{5}$$

where $\dot{N}$ is the particle delivery rate (s^{-1}), n is the particle density (m^{-3}), and A is the cross-sectional area of the pipe (m^2). The gas density ($n \sim \rho$) is obtained from the adiabatic relationships:

$$\frac{c}{c_0} = \left(\frac{T}{T_0}\right)^{\frac{1}{2}} = \left(\frac{\rho}{\rho_0}\right)^{\frac{\gamma-1}{2}} = \left(\frac{P}{P_0}\right)^{\frac{\gamma-1}{2\gamma}} \tag{6}$$

Thus for $t > \Delta t_0$, we can combine (2), (3), (5), and (6) to determine the particle delivery rate. Normalized to the reservoir conditions, this is given for monatomic ideal gases by:

$$\frac{(nu)_{x=L_\mathrm{p}}}{n_0 c_0} = \frac{3}{256}\left(1 + \frac{1}{t^*}\right)\left(3 - \frac{1}{t^*}\right)^3 \tag{7}$$

where $t^* \equiv t\,(c_0/L_\mathrm{p})$ is the normalized time, and $(nu)_{x=L_\mathrm{p}} \times A$ gives the rate of delivery of gas particles into the vacuum at $x = L_\mathrm{p}$.

For fixed hardware (A, L_p constant) and fixed reservoir gas pressure (n_0 constant), the particle delivery rate depends only on the gas sound speed at stagnation c_0. The normalized particle delivery rate given by (7), as well as the pipe exit velocity and pressure normalized to the plenum conditions, are shown graphically in figure 2. It can be seen that the particle delivery rate has a waveform that is about three times steeper versus time than the pipe exit pressure in the early phases of injection ($t^* \lesssim 1.5$). This is significant in that exit pressure is typically used as the (indirect) indicator of gas flow in experiments [13]. In particular, the particle delivery rate is $\sim 60\%$ of its steady-state value after one sonic transit time ($t = L_\mathrm{p}/c_0$), while the pressure has only reached $\sim 13\%$ of its steady-state value.

Taking the C-Mod case of $L_\mathrm{p} = 2$ m, the sonic transit times L_p/c_0 for helium ($c_0 \simeq 1000\ \mathrm{m\,s}^{-1}$) and argon ($c_0 \simeq 250\ \mathrm{m\,s}^{-1}$) are 2 ms and 8 ms, respectively. Given that the characteristic timescale for C-Mod disruption quenches is 1–2 ms, the importance of prompt gas delivery is obvious. In particular, it is important to realize that it is the initial delivery of gas (at $t = L_\mathrm{p}/3c_0$) that initiates the sequence leading to radiative termination (thermal quench). However, for the case of argon, the "bulk" of the gas is not delivered until more than 5 ms after this time. This is obviously undesirable with respect to maximizing the delivered particle inventory in the current quench. However, this limitation for argon delivery can be overcome by noting that the gas in the pipe is in a strongly viscous regime. Therefore, for small fractions of argon mixed with helium, the mixture can be treated as a single fluid with an effective atomic mass set by the admixture concentration of Ar with He. In such cases ($f_\mathrm{Ar} \lesssim 10\%$), the small concentration of argon will be delivered at nearly the same speed as for pure helium gas. The argon atoms are efficiently entrained with the helium and are delivered

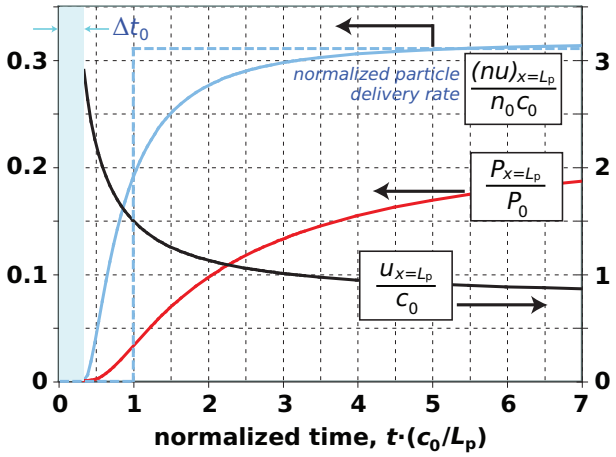

Figure 2. Normalized flow rate, pressure, and fluid velocity at the exit of a tube of length L_p for a reservoir gas of sound speed c_0. $\Delta t_0 = L_p/3c_0$ is the time at which the gas first arrives at the pipe exit.

at a much faster rate than is possible with pure Ar gas. The rapid delivery of the highly radiating argon brings advantages that will be explained in the following sections.

2.2. Energy removal

Although the fast delivery of species into the plasma is critical to mitigate the disruption, it is not enough by itself. The injected species must be effective at radiating away the plasma energy to prevent localized heat flux, and increase the electron density at the same time to prevent runaway formation. It has been shown [8] that high-Z impurities, having large radiation rate coefficients, can radiate the energy of the plasma efficiently. This is true even when they are injected in low quantities, as with killer pellets [14] or low-pressure gas puffing [10]. As a result, the radiative fraction of the stored thermal energy is higher with argon than with helium, as can be seen in figure 1(b). However, because of their slower particle delivery rate, high-Z impurities do not increase the electron density as effectively as does He. A high electron density is desirable for runaway suppression. A summary of density increments before the current quench with different noble gases is shown in figure 1(d). The highest density increments are obtained with helium; however, due to the low radiation rate of pure He, these injections are not as successful at mitigating the localized heat flux by radiative dissipation [8, 9].

If a mixture of mostly low-Z gas with small concentrations of high-Z gas can be delivered quickly to the plasma, it may remove the energy quickly and trigger the current quench earlier. The radiation power $P_{\rm rad}$ of a plasma contaminated with an impurity is approximately given by $P_{\rm rad} = n_{\rm e} n_{\rm z} L_{\rm z}$, where $n_{\rm e}$ is the free electron density, $n_{\rm z}$ is the number density of impurity atoms, and $L_{\rm z}$ is the radiation rate coefficient for the impurity. Thus injecting a mixture can lead to large radiation power densities even if the density of the high-Z mixture is low, because the ionization of the low-Z gas contributes many free electrons. One obtains a double benefit with the gas mixture:

the high-Z impurities arrive more quickly due to their viscous transport by the low-Z carrier gas, and the efficiency of the radiation is improved by the electrons contributed by the ionization of the carrier gas.

2.3. Resistive termination

After the thermal quench, poloidal halo currents become a concern. These can be decreased by increasing the current quench rate [15]. After the thermal quench, the plasma temperature, and hence resistivity and CQ rate, are determined primarily by the the ionization energy of the injected gas. This is because the plasma is in equilibrium between ohmic heating and line radiation [3]. This can be seen in figure 1(c). In the case of mixed gas species, it the species with the lowest ionization potential will primarily set the temperature. In the case of helium-argon mixtures, then, it is expected that Ar (ionization energy 16 eV) will dominate over He (ionization energy 24 eV). This holds even if the argon is a small fraction of the helium, due to the exponential sensitivity of ionization rate to temperature when the temperature is below the ionization energy. We therefore expect the gas mixture to cause a reduction in halo current, similar to that found with pure argon, even at low admixture fractions.

3. Experimental setup and observations

The gas jet disruption mitigation system on Alcator C-Mod consists of a 300 mL high-pressure plenum that is typically filled to 7 MPa with a noble gas. A fast-response valve, located at the plenum, delivers the gas into a connecting pipe of 2 m length, and 9.4 mm internal diameter. The valve is open for approximately 1.3–2.0 ms. Technical details of the disruption mitigation system are presented in [8]. Disruption mitigation experiments using mixed gases were performed during four runs in 2006, 2007, and 2009.

The 2006 experiments began with pure He injection on the first shot. Then, after each shot, the plenum was refilled *in situ* using a 50% He + 50% Ar gas mixture. This gradually increased the Ar fraction of the plenum, allowing us to do a scan of Ar concentrations in a single run. The actual fractions of species were measured using a residual gas analyzer. The main target plasma parameters were $I_\mathrm{p} = 1.2$ MA, $n_\mathrm{e0} \sim 10^{20}$ m^{-3}, and $B_\mathrm{t} = 5.4$ T. Further experiments were performed in 2007 and 2009 using an 85% He + 15% Ar gas mixture as well as mixtures of 85% D_2 + 15% Ar and 85% He + 15% Kr into a target plasma with $I_\mathrm{p} = 1.0$ MA, $n_\mathrm{e0} \sim 10^{20}$ m^{-3}, and $B_\mathrm{t} = 5.5$ T.

In figure 3 we show waveforms of the electronic trigger to the valve, the pressure rise at the pipe inlet (just downstream from the high-pressure plenum), the central soft X-ray signal from the plasma, and plasma current for typical diruption mitigation experiment using a mixture of 88% He + 12% Ar. The valve opens, indicated by the rising pressure ~ 2 ms after the command is given to the valve, and inlet pressure quickly approaches steady state. After a delay time, set by the gas delivery speed and radiation efficiency, the core temperature collapses (indicated by soft X-ray emission), and the plasma current resistively decays. The timing of this sequence is highly reproducible (variation < 0.1 ms) if the target plasma and injection gas type and pressure are kept

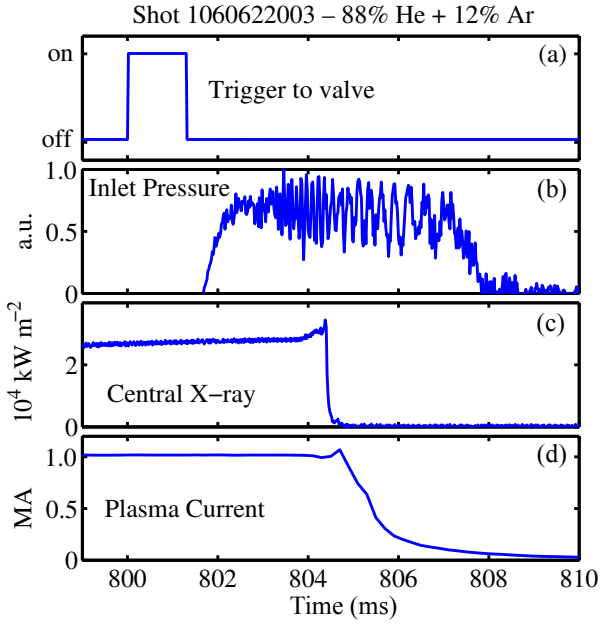

Figure 3. Waveforms for C-Mod shot 1060622003, a typical disruption mitigation experiment using a mixture of 88% He + 12% Ar. (a) Current applied to the valve, (b) pressure at the valve outlet, (c) central soft X-ray intensity, (d) plasma current.

constant.

Waveforms of edge soft X-ray intensity, plasma current, poloidal halo current, and line-integrated electron density for for disruption mitigation shots using 100% He, a mixture of 90% He + 10% Ar, and a mixture of 50% He + 50% Ar are shown in figure 4. Edge soft X-ray signals, as a qualitative measure of temperature, show simultaneous thermal quenches with pure He and a mixture of 90% He + 10% Ar. This indicates that the pure He gas and the 90% He + 10% Ar mixture gas front arrives at the plasma column at approximately the same time. The thermal quench with 50% He + 50% Ar starts approximately 2 ms later than for the others, indicating a lower gas front velocity, as would be expected from the increase in effective atomic mass. However, the current quench with 90% He + 10% Ar starts $\sim$ 1 ms earlier than with pure He, indicating improved radiation efficiency. The electron density increment with the mixture at the early phase of injection nearly overlaps with that of pure He. Poloidal halo currents are smallest with the 90% He + 10% Ar mixture. These observations are all consistent with expectations for low-fraction admixtures of high-Z gas, as discussed in section 2. In the following subsections we explore these observations in detail.

3.1. Gas delivery speed

The time of the start of the thermal quench (indicated by the delay between the start of the pressure rise at the valve and the collapse of the edge soft X-ray signal on SXR chords 5, 6, and 7, at $r/a = 0.96$, 0.91, and 0.87 respectively) is plotted versus the sound speed for several gas mixtures in figure 5. Also shown is the signal from when radiation was first observed on a fast ultraviolet diode pointing at the gas jet [16]. It

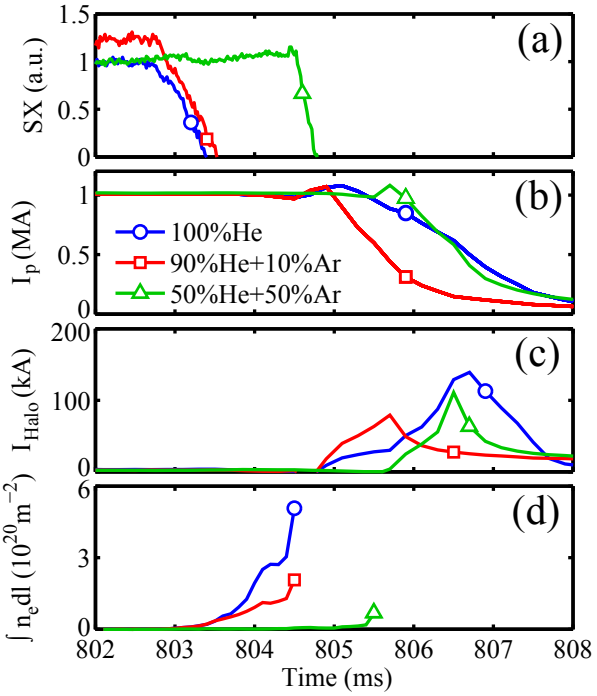

Figure 4. Waveforms of (a) edge soft X-ray signal, (b) plasma current, (c) halo current, (d) chord-integrated electron density for 3 disruption mitigations using pure helium (blue circle), a mixture of 90% He + 10% Ar (red square), and a mix of 50% He + 50% Ar (green triangle).

can be seen that the gas arrives at the plasma at a time very close to the predicted time $\Delta t_0 = L_\mathrm{p}/3c_0$, but that the edge soft X-ray collapse is delayed by a time known as the pre-thermal quench (pre-TQ) time [17]. The mixture of 15% Ar + 85% D_2 used in one set of MGI experiments has a specific heat ratio $\gamma \simeq 1.44$ and thus the shock arrives after a delay $\Delta t_0 \simeq 0.22 L_\mathrm{p}/c_0 = 0.7$ ms, more quickly than for the mixtures of monatomic ideal gases.

The time of the start of the thermal quench and the arrival of the gas at the plasma is shown in figure 6 for just the argon/helium mixtures. It can be seen that the time the gas takes to arrive at the plasma increases as the sound speed of the gas decreases.

3.2. Thermal quench and radiation power

As discussed in section 2.2, the ability of the gas to effectively radiate the plasma energy away during the thermal quench is critical to prevent localized heat loads to plasma facing components. The time-integrated radiation power during the thermal quench versus the argon fraction for a series of Ar/He disruption mitigation shots is shown in figure 7(a). As expected, the lowest radiated energy is seen for pure helium. In all of these shots, total stored energy (thermal + poloidal magnetic energy) is approximately 0.65 MJ. The radiation power increases with the fraction of argon in the mixture, up to an argon fraction of approximately 10%. For larger fractions, the

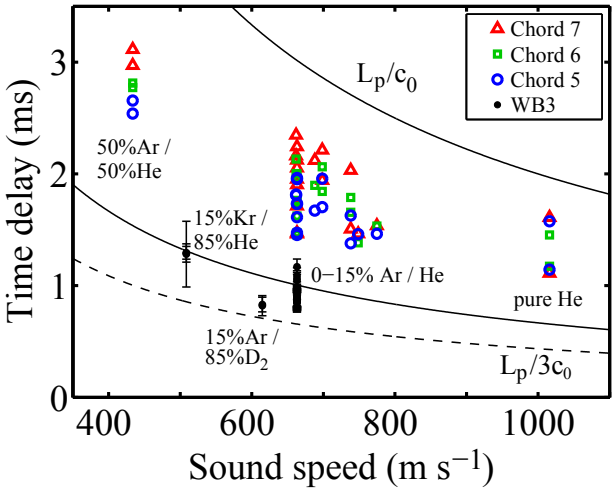

Figure 5. The time of the collapse of the edge soft X-ray signals correlates with the time of the arrival of the gas to the plasma for a variety of gas mixtures. Blue circles: chord 5 (r/a = 0.96), green squares: chord 6 (r/a = 0.91), red triangles: chord 7 (r/a = 0.87). A fast photodiode ("WB3") pointing directly at the gas jet [16] indicates the arrival of the gas at the plasma. Error bars are monte carlo estimates from fits to the break in slope of the WB3 signal and the rise of the pressure transducer. The solid lines indicate the modelled gas arrival time $L_p/3c_0$ and the sonic transit time L_p/c_0. The mixture of 15% Ar + 85% D_2 has a specific heat ratio $\gamma \simeq 1.44$ and thus the shock arrives after a delay $\Delta t_0 \simeq 0.22 L_p/c_0 = 0.7$ ms. This is indicated by a dashed line.

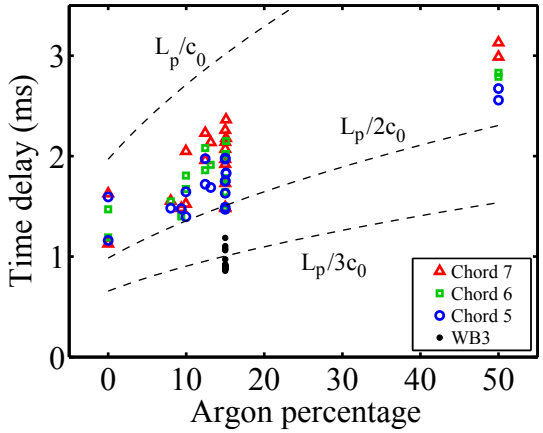

Figure 6. The time of the collapse of the edge soft X-ray signals correlates with the time of the arrival of the gas to the plasma for argon/helium mixtures. Blue circles: chord 5 (r/a = 0.96), green squares: chord 6 (r/a = 0.91), red triangles: chord 7 (r/a = 0.87). A fast photodiode pointing directly at the gas jet [16] indicates the arrival of the gas at the plasma. Dashed lines indicate the modelled gas arrival time $L_p/3c_0$ and the sonic transit time L_p/c_0.

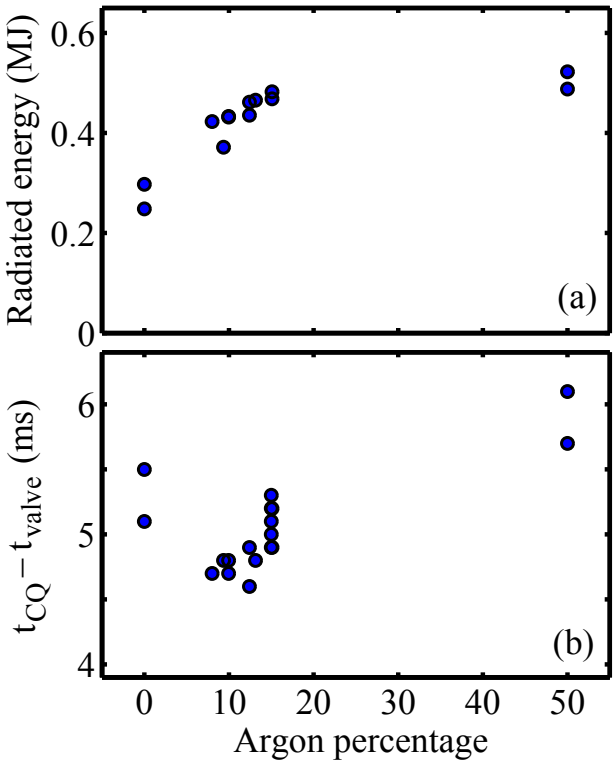

Figure 7. Radiated energy during thermal quench and delay time from signal sent to valve, to start of current quench, for mixtures of argon/helium. (a) For argon fractions less than approximately 20%, the radiated energy during the thermal quench increases with the argon fraction. (b) The delay to the start of the current quench is a minimum for argon fractions of approximately 10–15%.

radiation power is nearly constant.

In figure 7(b), the time elapsed from the triggering signal being sent to the disruption mitigation valve to the start of the current quench (defined as the maximum measured plasma current) is shown for the same series of Ar/He discharges. This delay time reaches a minimum for argon fractions of 10–15%. This demonstrates the advantages of gas mixtures: high radiation efficiency with a fast global response time.

The density increment before the current quench is particularly important for runaway electron suppression. The free electron density measured during 3 disruption mitigation experiments using He/Ar mixtures in C-Mod is shown in figure 4(d). The highest density increment is obtained with pure helium and the lowest with the 50% He + 50% Ar mixture. These signals show the free electron density in the plasma. However, for runaway electron suppression, it is the *total* electron density $n_{e,T}$ (including bound electrons) that is significant. There exists no measurement technique for the total electron density, and therefore we have investigated $n_{e,T}$ using the KPRAD 0-D transport code in section 4.2.

3.3. Current quench and resistivity

The halo currents measured during the experiments are shown in figure 8(c) for

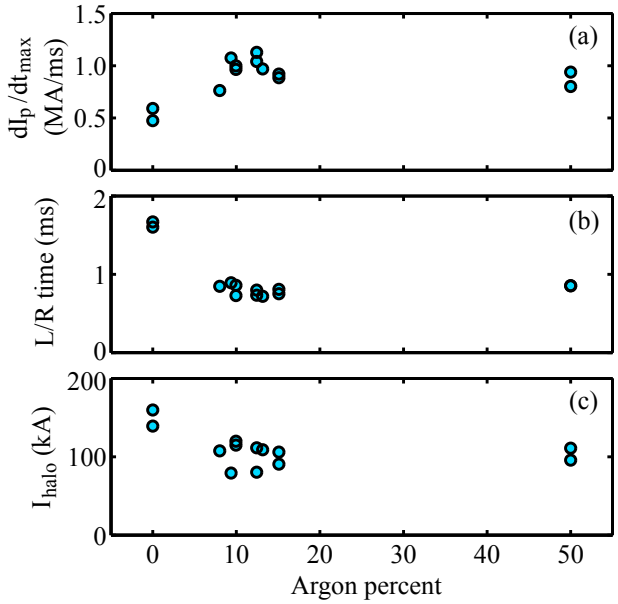

Figure 8. (a) Helium/argon mixtures with low argon fractions produce the maximum current quench rates. (b) The L/R current-decay timescale in all Ar/He mixtures is lower than that in pure helium, and consequently the peak halo current (c) is lower using gas mixtures.

helium/argon gas mixtures. The highest halo current is observed during pure He injections, although this is still an improvement from unmitigated VDE disruptions with $I_{\rm halo} \sim 225$ kA. This is consistent with previous experimental observations [8]. All mixtures lead to lower halo current than with pure He. However, there is little additional reduction in halo current for argon fractions above 10%. This is consistent with the physical picture presented in section 2.2 – the argon dominates the thermal balance of the CQ plasma even at low admixture fractions.

4. Discussion

We have used a simple 0-D transport code with energy balance (KPRAD) to calculate the response of a plasma with similar experimental parameters to the target plasmas used in the disruption mitigation experiments. The flow rate of the injected species is obtained from the analytical equations given in section 2.1. There are no free parameters in the calculation.

4.1. Gas delivery speed

In section 3.1 we used the soft X-ray signals at the edge (chords 5–7) as an indication of the time when the radiation power from the injected gas species has become much higher than the ohmic power. A fast photodiode looking directly at the gas jet showed that the actual arrival of the gas at the plasma was described well by the analytic model presented in section 2.1.

As can be seen in figure 5, the timing of the soft X-ray collapse correlates with the time when the gas arrives at the plasma, although with a different numerical coefficient

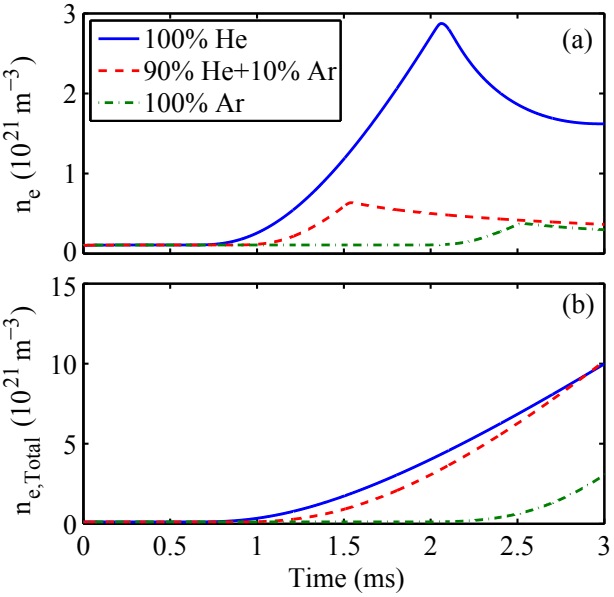

Figure 9. (a) The simulated free electron density agrees well with the experimental results (see figure 4d). In the case of helium-argon gas mixtures, the contribution of the argon to the density increment is $\sim 20\%$. (b) Similar total (free + bound) electron density is obtained using pure He and 90% He + 10% Ar.

($\Delta t_{\mathrm{SXR}} \sim L_{\mathrm{p}}/2c_0$). This difference is likely due to the time required for the gas injection to accumulate to sufficient density in the plasma to cause the edge plasma to suddenly cool. The delay from the arrival of the gas at the plasma to the onset of the thermal quench is discussed further in [17]. For analyzing the flow rate of gas mixtures, (7) is adequate.

4.2. Thermal quench and radiation power

In figure 5 it was shown that the thermal quench starts earlier using mixtures with higher sound speeds. The second critical requirement for disruption mitigation is the electron density increment. The free electron density increment gives a qualitative indication of the particle delivery; however, it is the total electron density (free + bound) which is required for suppression of runaway electrons. The results of a 0-D simulation are shown in figure 9, with results similar to the experimental data (figure 4). Figure 9(b) shows an interesting result: the total electron density is with 90% He + 10% Ar is nearly identical to that from pure He injection, despite the total delivered atoms with 90% He + 10% Ar being low. The contribution of the argon in increasing the total electron density in the 90% He + 10% Ar mixture is approximately 20%. The total electron density with 50% He + 50% Ar is very low during the thermal quench (see figure 4(d)).

4.3. Current quench and resistivity

The 0-D KPRAD code was also used to calculate the plasma resistivity immediately after the thermal quench for simulated injections of helium-argon mixtures. The

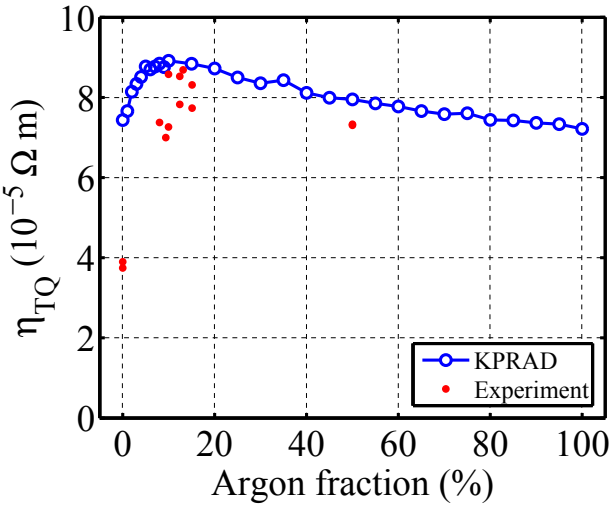

Figure 10. Observed (from current decay L/R timescale) and calculated (KPRAD) resistivity of the plasma immediately after the thermal quench, for helium-argon mixtures. Using a mixture of approximately 15–20% Ar forces the plasma to a highly resistive phase.

experimental post-TQ resistivity was calculated from the observed R/L current decay timescale during the current quench. The two are compared in figure 10. There are no free parameters in the KPRAD model. Agreement is better for gas mixtures than for pure helium due to (explanation).

5. Conclusions

Helium-argon and other gas mixtures were used in disruption mitigation experiments on Alcator C-Mod to investigate the advantages of mixtures versus single-species injections. Through comaprison to pure-gas experiments and numerical calculations, the following results have been obtained:

- The speed of gas delivery for a variety of gas mixtures is well described by assuming that the gas mixture is in a highly viscous regime, and acts as a single gas with an effective sound speed set by the effective atomic mass and adiabatic constant for the mixture.
- Helium-argon mixtures with a low argon fraction approach the plasma at nearly the same speed as pure helium. They produce a similar total (free + bound) electron density increment, which is critical to suppress runaway electrons.
- The radiation power and current quench time using helium-argon mixtures are similar to those when using pure argon. Halo currents are mitigated for pure Ar and He-Ar mixtures.
- Helium-argon mixtures trigger the current quench faster than pure helium or pure argon.
- Intrinsic impurities appeared to contribute less to the radiation power than with pure helium injection.

Acknowledgments

This work was supported by the U.S. Department of Energy under grant number DE-FG02-04ER54762 and U.S. DOE Cooperative Agreement DE-FC02-99ER54512. Additional support was provided by the Natural Sciences and Engineering Research Council of Canada PGS M program.

References

[1] T.C. Hender, J.C. Wesley, J. Bialek, A. Bondeson, A.H. Boozer, R.J. Buttery, A. Garofalo, T.P Goodman, R.S. Granetz, Y. Gribov, O. Gruber, M. Gryaznevich, G. Giruzzi, S. Gunter, N. Hayashi, P. Helander, C.C. Hegna, D.F. Howell, D.A. Humphreys, G.T.A. Huysmans, A.W. Hyatt, A. Isayama, S.C. Jardin, Y. Kawano, A. Kellman, C. Kessel, H.R. Koslowski, R.J. La Haye, E. Lazzaro, Y.Q. Liu, V. Lukash, J. Manickam, S. Medvedev, V. Mertens, S.V. Mirnov, Y. Nakamura, G. Navratil, M. Okabayashi, T. Ozeki, R. Paccagnella, G. Pautasso, F. Porcelli, V.D. Pustovitov, V. Riccardo, M. Sato, O. Sauter, M.J. Schaffer, M. Shimada, P. Sonato, E.J. Strait, M. Sugihara, M. Takechi, A.D. Turnbull, E. Westerhof, D.G. Whyte, R. Yoshino, H. Zohm, and the ITPA MHD and Disruption and Magnetic Control Topical Group. Chapter 3: MHD stability, operational limits and disruptions. *Nuclear Fusion*, 47(6):S128–S202, June 2007.

[2] R. Yoshino, Y. Neyatani, N. Isei, Y. Koide, Y. Kawano, A. Tanga, D.J. Campbell, M.F. Johnson, and L. Rossi. Disruption amelioration experiments in JT-60U and JET. In *Proceedings of the 15th International Conference on Plasma Physics and Controlled Nuclear Fusion Research, Seville, Spain, September 26–October 1, 1994*, volume 1, pages 685–695. IAEA, 1995.

[3] D.G. Whyte, T.C. Jernigan, D.A. Humphreys, A.W. Hyatt, C.J. Lasnier, P.B. Parks, T.E. Evans, M.N. Rosenbluth, P.L. Taylor, A.G. Kellman, D.S. Gray, E.M. Hollmann, and S.K. Combs. Mitigation of tokamak disruptions using high-pressure gas injection. *Physical Review Letters*, 89(5), July 29 2002.

[4] V.A. Izzo. A numerical investigation of the effects of impurity penetration depth on disruption mitigation by massive high-pressure gas jet. *Nuclear Fusion*, 46(5):541–547, May 2006.

[5] R.W. Harvey, V.S. Chan, S.C. Chiu, T.E. Evans, M.N. Rosenbluth, and D.G. Whyte. Runaway electron production in DIII-D killer pellet experiments, calculated with the CQL3D/KPRAD model. *Physics of Plasmas*, 7(11):4590–4599, November 2000.

[6] M. Bakhtiari, G.J. Kramer, M. Takechi, H. Tamai, Y. Miura, Y. Kusama, and Y. Kamada. Role of bremsstrahlung radiation in limiting the energy of runaway electrons in tokamaks. *Physical Review Letters*, 94(21), June 2005.

[7] K.H. Finken, G. Mank, A. Krämer-Flecken, and R. Jaspers. Mitigation of disruptions by fast helium gas puffs. *Nuclear Fusion*, 41(11):1651–1661, November 2001.

[8] R. Granetz, D.G. Whyte, V.A. Izzo, T. Biewer, M.L. Reinke, J. Terry, A. Bader, M. Bakhtiari, T. Jernigan, and G. Wurden. Gas jet disruption mitigation studies on Alcator C-Mod. *Nuclear Fusion*, 46(12):1001–1008, December 2006.

[9] M. Bakhtiari, H. Tamai, Y. Kawano, G.J. Kramer, A. Isayama, T. Nakano, Y. Kamiya, R. Yoshino, Y. Miura, Y. Kusama, and Y. Nishida. Study of plasma termination using high-Z noble gas puffing in the JT-60U tokamak. *Nuclear Fusion*, 45(5):318–325, May 2005.

[10] M. Bakhtiari, Y. Kawano, H. Tamai, Y. Miura, R. Yoshino, and Y. Nishida. Fast plasma shutdown scenarios in the JT-60U tokamak using intense mixed gas puffing. *Nuclear Fusion*, 42(10):1197–1204, October 2002.

[11] M. Bakhtiari, R. Yoshino, and Y. Nishida. Fast thermal shutdown of tokamak discharges without runaway electron avalanching. *Fusion Science and Technology*, 41(2):77–87, March 2002.

[12] I.I. Glass and J.P. Sislian. *Nonstationary flows and shock waves*. Oxford University Press, 1994. pp. 28–29.

[13] T.C. Jernigan, L.A. Baylor, S.K. Combs, D.A. Humphreys, P.B. Parks, and J.C. Wesley. Massive gas injection systems for disruption mitigation on the DIII-D tokamak. In *Fusion Engineering 2005, Twenty-First IEEE/NPSS Symposium on, Knoxville, TN, USA, September 26–29, 2005*, pages 1–3. IEEE/NPSS, 2005.

[14] R. Yoshino, T. Kondoh, Y. Neyatani, K. Itami, Y. Kawano, and N. Isei. Fast plasma shutdown by killer pellet injection in JT-60U with reduced heat flux on the divertor plate and avoiding runaway electron generation. *Plasma Physics and Controlled Fusion*, 39(2):313–332, February 1997.

[15] V. Riccardo, P. Barabaschi, and M. Sugihara. Characterization of plasma current quench at JET. *Plasma Physics and Controlled Fusion*, 47(1):117–129, January 2005.

[16] M.L. Reinke, D.G. Whyte, R. Granetz, and I.H. Hutchinson. Toroidally resolved radiation dynamics during a gas jet mitigated disruption on Alcator C-Mod. *Nuclear Fusion*, 48, November 2008.

[17] Matthew Reinke, Robert Granetz, Ian Hutchinson, and Dennis Whyte. 3-D radiation dynamics during gas jet mitigated disruptions on Alcator C-Mod. In *51st Annual Meeting of the APS Division of Plasma Physics, Atlanta, GA, USA, November 2–6, 2009*. APS/DPP, 2009. Abstract ID BAPS.2009.DPP.UO4.3.